

Seeing the Ocean through Sea Ice

Robert A Fajber

November 15, 2017

Abstract

Signatures of submesoscale ocean filaments are commonly observed in satellite images of thin, sparse sea ice. However, sea ice is not a passive tracer, and its distribution over regions of surface ocean convergence depends on a balance between the external ocean drag and the internal stresses due to ice-floe interactions. Therefore, the distribution of sea ice thus depends on ice-ocean interactions at the submesoscale.

This study looks at two idealized cases. The first is a convergent filament with surface flow that is independent from the sea-ice. Sea ice accumulates over the center of the filament, and shows multi-timescale behavior. The second case is a filament where the surface flow is driven by ocean dynamics through Ekman transport. It is shown that the coupled ice-ocean system is able to accumulate sea-ice for certain rheological regimes.

The results of these two idealized test cases show that concentrations of sea ice over filaments are able to develop on timescales of 1-2 days, and that the peak of the concentration profile can be several times the background. This gives an indication that snapshots of sea ice could be used to constrain surface ocean currents.

1 Motivation

Upper ocean dynamics contains a rich array of submesoscale eddies and filaments with high Rossby numbers and scales below the Rossby deformation radius, resulting from mixed layer and submesoscale instabilities [9]. Submesoscale currents can frequently develop energetic ageostrophic vertical velocities. This provides a mechanism of vertical tracer transport across the mixed layer that is critical for biogeochemical processes in the ocean [6] and also creates strong vertical heat fluxes. In addition, submesoscale eddies provide a mechanism for the forward energy cascade towards dissipation (contrary to mesoscale dynamics, which leads to energy cascade to large scales). Understanding submesoscale dynamics as it relates to upper ocean tracer transport, modification of surface buoyancy fluxes, and energy cycles remains a long-standing problem in oceanography.

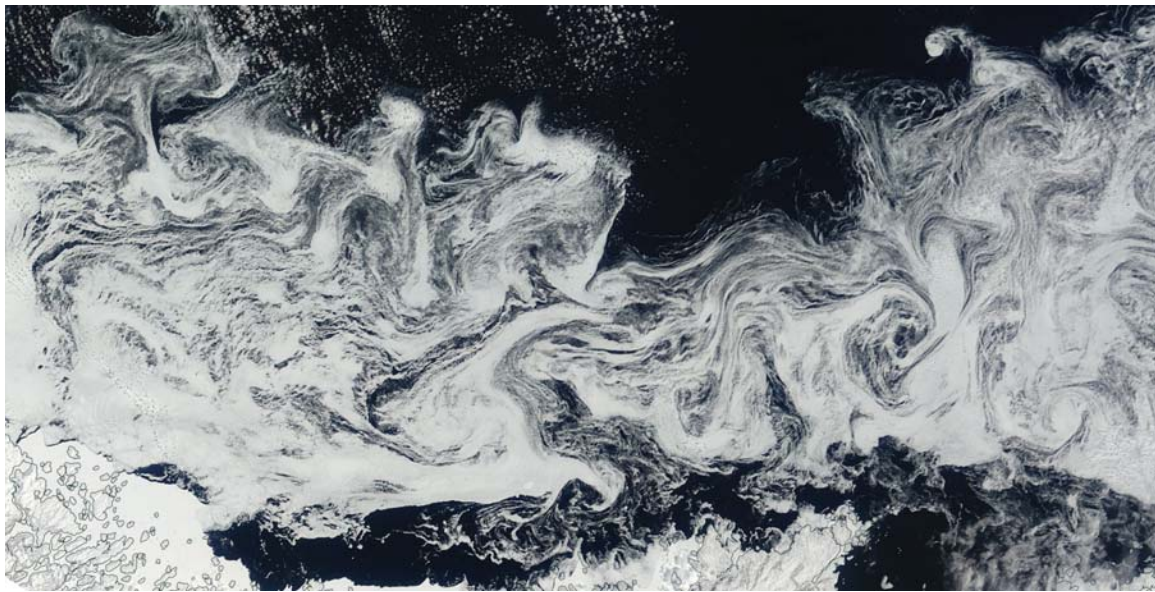


Figure 1.1: Satellite reflectance image (Aqua/MODIS) of sea ice in the marginal ice zone in the Labrador sea, taken from NASA Worldview: <https://worldview.earthdata.nasa.gov/>. Image resolution is 250 m and total width is about 400 km with eddy sizes $O(20 \text{ km})$ and filament widths $O(5 \text{ km})$. The Labrador coastline is visible in the bottom of the photograph, and small clouds are visible at the top of the photograph.

Satellite observations of ocean altimetry and sea ice are limited to the larger, geostrophically constrained scales [2]. Making *in situ* observations in the polar oceans is particularly complicated due to the presence of sea ice and icebergs, which can destroy instruments [1]. As a result, studies of submesoscale currents in the polar oceans are limited to relatively few observations [13]. Under the heavily packed multi-year sea ice, the submesoscale variability is significantly damped since ice acts as a momentum and energy sink for upper ocean flows [10]. However, submesoscale variability is energetic in marginal ice zones and can substantially enhance the ocean-ice heat source by bringing warm sub-mixed layer waters in contact with the ice [8].

At sufficiently low concentrations, the sea ice can accumulate in convergent surface ocean currents creating submesoscale concentration patterns visible from satellite images [8], see figure 1.1 for example. The sea ice accumulation is opposed by internal ice stresses, leading to a quasi-steady balance with elevated sea ice concentrations over converging cyclonic eddies and filaments. Identifying conditions favorable for pattern formation in sea ice is complicated by the fact that the sea ice rheology is still largely unknown [3]. Yet, satellite images of marginal ice zones suggest that ice concentrations are indeed tightly related to the divergence patterns of the underlying ocean currents.

Here, we present a theoretical framework to explain the development of sea ice concentration patterns over idealized ocean eddies and filaments. Throughout this work we prioritize analytical tractability over rheological complexity by retaining only the very critical aspects of sea ice rheology, with the goal of elucidating the key physical balances. The report is organized as follows: In Section 2 we derive an idealized model of sea ice evolution driven by converging upper ocean flow. In Section 3 we apply the model to a cyclonic filament that has a strong ageostrophic surface flow resulting in sea ice accumulation. In Section 4 we explore sea ice accumulation over near-geostrophic flows where it is the presence of sea ice (and a corresponding ice-ocean stress) that generates the Ekman convergence. In Section 5 we discuss potential applications of our theoretical framework to estimating the statistical properties of upper-ocean divergence field from still images of sea ice concentration.

2 Equations of Sea Ice Motion

2.1 Development of equations

The model that we use treats sea ice as a continuous media, similar to [4, 11]. The development of the model follows a standard approach for the fluid dynamics of a continuum mixture, which we review below to introduce the key assumptions made.

Although sea ice is composed of individual floes that strongly interact with each other, we assume that the the dynamics can be averaged over a sufficiently large scale that the properties of the floes (e.g. floe-floe stresses) can be represented using

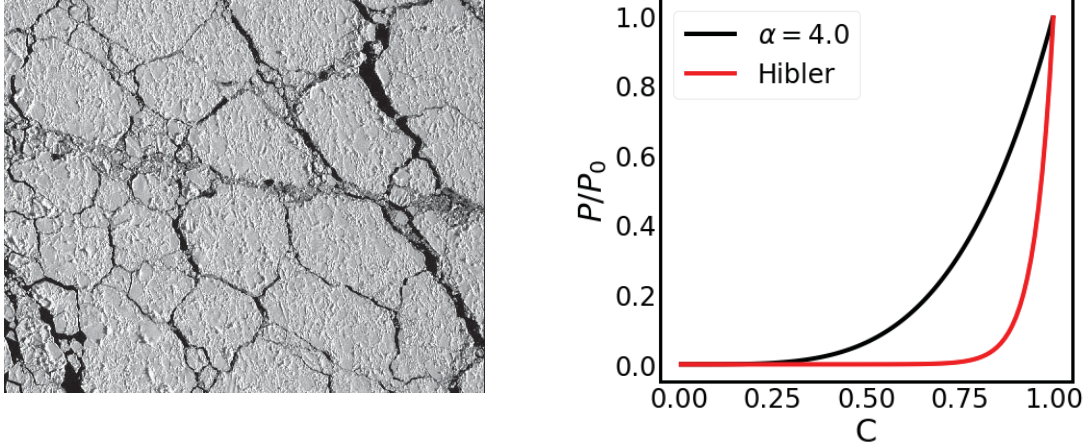


Figure 2.1: (a) Distribution of sea ice (with dark areas representing open ocean) emphasizing strong interactions between individual ice floes (with characteristic diameters of about 100 m). The ice occupies an area A_I within a total image area A , over which the sea ice is considered as a continuous media (see Eq. 2.4 and discussion in the text). Taken from [7]. (b) The continuous power-law ‘equation of state’ showing the critical dependence of sea ice pressure on concentrations (black). The Hibler rheology [4] is shown in red for comparison.

average properties (e.g. the concentration and average velocity). Our study will focus only on the dynamic equations of sea ice motion, since on submesoscale timescales (order of days to a week), much shorter than the sea ice thermodynamic timescale of several months [11], justifying the neglect of the sea ice.

We assume that the ice within some region A has a uniform thickness h and covers an area A_I , a typical sea ice state is shown in Fig. 2.1a. The resulting concentration $C(\mathbf{r}, t) = A_I A^{-1}$ can evolve in time and space. We consider purely two-dimensional ice motion along the ocean surface with sea ice velocities $\underline{u} = (u, v)$ that may be divergent. Dividing the mass conservation equation by A yields

$$0 = \partial_t \int_V \rho C dV + \int_V \rho \nabla \cdot (C \underline{u}) dV,$$

where ρ is the density of the ice. Doing this integral and noting that the vertical component vanishes, and dividing by ρh gives the concentration evolution equation

$$0 = \partial_t (C) + \nabla \cdot (\underline{u} C), \quad (2.1)$$

with $\nabla = (\partial_x, \partial_y)$. We note that $C \in [0, 1]$, but this constraint is not enforced by equation 2.1. If a system produces $C > 1$, then this corresponds to a breakdown of model physics, implying that the assumption of constant height is broken.

Assuming that the ice has negligible inertia, the conservation of momentum equation

can be written as a balance between the internal, $\underline{\tau}_{int}$, and external stresses $\underline{\tau}_{ext}$,

$$0 = \oint_S (\underline{\tau}_{ext} + \underline{\tau}_{int}) \cdot d\underline{S}, \quad (2.2)$$

where S is the surface of V . To simplify the external stress we assume

- $\underline{\tau}_{ext} = 0$ except on the top and bottom surfaces.
- $\underline{\tau}_{ext}$ acts only on the sea ice .
- $\underline{\tau}_{ext}$ is constant on the lower surface of S .

Taken together these assumptions give

$$A^{-1} \int_S \underline{\tau}_{ext} \cdot d\underline{S} = C \underline{\tau}_w, \quad (2.3)$$

where $\underline{\tau}_w$ is the water stress on the bottom surface of the ice. We note that there is also an atmospheric force acting on the top of the ice in principle, but we will ignore it here since the focus of the project is on the interaction of the ice and the ocean. To simplify the internal stress we assume that:

- $\underline{\tau}_{int}$ parameterizes collisions between sea ice on the boundary of V .
- $\underline{\tau}_{int}$ is independent of z ,

so that

$$\begin{aligned} \oint \underline{\tau}_{int} \cdot d\underline{S} &= \int_V \nabla \cdot \underline{\tau}_{int} dV \\ &= h \int_A \nabla \cdot \underline{\tau}_{int} dA. \end{aligned} \quad (2.4)$$

To understand why the integral involving τ_{int} appears as a boundary term, consider an ensemble of interacting floes in an area A . If there are no other forces other than the collisions between floes, then the total force acting on all the floes must be 0, since by Newton's third law every collisional force will have an equal and opposite force. If the area A is subdivided into two areas, A_1 and A_2 , then the total force on the sea ice inside area A_1 will be due to collisions between floes in A_1 and A_2 , since collisions between floes only in A_1 will cancel. Thus, the interactions which can exert a force on an ensemble of floes are interactions that involve floes from another ensemble. If we consider the ensembles of floes to be in neighboring areas, then the only place for these floes to interact is at the boundary of the area that we are averaging over.

Since this internal stress represents the average statistical properties of the collisions within the area A , then they have to be evaluated over the entire boundary. After applying the divergence theorem, this is equivalent to saying that they have to be integrated over the entire volume. This is different than the external stress, which only acts on the surface of the sea ice, hence the factor of C difference between the two terms.

The internal stress can be further separated into an isotropic component including a pressure P that we assume only depends on the concentration of ice, and a deviatoric stress $\underline{\sigma}$:

$$\underline{\tau}_{int} = -P\underline{I} + \underline{\sigma}. \quad (2.5)$$

By assuming that the area A is arbitrary and combining equations (2.2)-(2.5), we find

$$0 = C\underline{\tau}_w - h [\nabla P + \nabla \cdot \underline{\sigma}]. \quad (2.6)$$

2.2 Simplified sea ice rheology

To complete the system we have to specify a drag law for $\underline{\tau}_w$, an equation of state for P and an equation for $\underline{\sigma}$. Our choices for this are motivated by the physics governing the system, but we have also made additional simplifications to allow for a more tractable mathematical analysis. Our final system differs therefore from other more complicated models (for example the Hibler model [4]) that include more terms in the momentum equation in order to have simulations that are realistic enough to compare to large scale observations of thick, high concentration sea ice.

We assume that the drag law can be linearized so that

$$\underline{\tau} = -\rho_w \Gamma_d (\underline{u} - \underline{u}_w) \quad (2.7)$$

where ρ_w is the density of water, and Γ_d is a drag coefficient with units ms^{-1} , and \underline{u}_w is the water velocity.

The pressure term includes the large scale effect of collisions between individual ice floes. To include this we use an 'equation of state' which describes the pressure as a function of the concentration. This means that a concentration gradient in the ice will create a force on the ice due to internal stresses. Physically, this corresponds to there being more collisions in a region with high ice concentration and fewer collisions in a region with low ice concentration, with the result of an average force towards the region with lower concentration (the intuition here is similar to an ideal gas, hence the comparison with the equation of state). In principle, the equation of state should be determined by either detailed field measurements or by consideration of a model of sea ice floe collisions. In this study however, we will pick a form that matches our physical intuition, namely that at low concentrations the pressure should become

very small, and at concentrations approaching 1 the pressure should become very large, with a sharp transition in between. We also choose a form that is convenient for analytical analysis. One form that accomplishes these goals is

$$P = P_0 C^\alpha, \quad (2.8)$$

In this study we choose $\alpha = 4$; note that the choice $\alpha = 4$ corresponds to the dynamics of a thin viscous film (see section 3 in [14]). The choice of the rheology is essentially arbitrary. The rheology of [4] is chosen on the basis of observational comparison with wintertime ice distributions. The function is somewhat arbitrary – the only real constraints are the ones mentioned in the previous section. Our choice of a power law gives a good qualitative comparison to the rheology of [4], but is more analytically tractable, allowing us to advance our analysis further.

We specify the deviatoric stress by assuming that the fluid behaves like a Newtonian fluid so that

$$\underline{\underline{\sigma}} = \eta \left(\nabla \underline{u} + (\nabla \underline{u})^T \right) \quad (2.9)$$

where the viscosity η is a constant. This approximation is a significant simplification compared to the physical nature of sea ice, which is thought to behave as a shear thinning fluid [3]. Other models have assumed that ice can be treated either as a visco-plastic material [4], or an elastic-visco-plastic material [5] where the elasticity is introduced for numerical convenience. However, in these models it is found that the ice usually goes between the two extremes, either as a plastic fluid at high concentrations or as a viscous fluid at low concentrations. Since we are primarily interested in the low concentration limit with high shear, the Newtonian approximation should be valid in this region. In section 4 we will also take both the $\eta \rightarrow 0$ and the $\eta \rightarrow \infty$ limits of the system to further understand the implications of this choice.

Equations (2.1), (2.6), (2.7), (2.8), and (2.9) are a closed set of equations that can be solved to find the time varying ice concentration field. In the geometry of our problems, we will only be interested in motion that varies in one direction, which we will take to be y . We can substitute equations (2.7), (2.8), and (2.9) into equation (2.6) and simplify all the equations by eliminating terms involving ∂_x to get

$$\begin{aligned} \partial_t C &= -\partial_y(vC), \\ 0 &= -C\rho_w\Gamma_d(v - v_w) - hP_0\partial_y C^\alpha + \eta\partial_y^2 v, \\ 0 &= -C\rho_w\Gamma_d(u - u_w) + \eta\partial_y^2 u. \end{aligned} \quad (2.10)$$

2.3 Comment on assumptions

Throughout the development of the model we have made several assumptions to simplify the theory, some of which have been made for mathematical expediency. In deriving equations (2.1) and (2.6), it was assumed that the distribution of floe sizes was irrelevant. If the distribution of floe thicknesses and sizes is important, an additional equation that constrains the distribution (like the thickness equation)

would have to be added. This would also add a meaningful constrain on C , as well to constrain it to be $C \in [0, 1]$.

Atmospheric drag is removed primarily for the sake of simplicity. At the scales below 1km, atmospheric drag is highly variable. At the larger scale, the atmospheric drag can be very important for the sea ice distribution, but the scales are much larger than the ones here. During strong atmospheric storms, the atmospheric drag destroys all of the structure described in this study. For instance, atmospheric arctic mesocyclones referred to as "polar lows" can reach hurricane force winds, but typically have horizontal scales of 100-500km [12]. Atmospheric drag at much smaller scales could also create deviations from a purely ocean-driven sea ice distribution while not completely removing all of the structures inherited from the ocean currents. Ignoring the atmospheric drag thus restricts us to using the model on relatively calm days, with weak atmospheric drag.

The choices of the sea ice rheology are not expected to make a large difference compared to Hibler's model [4] and are primarily done for the sake of mathematical tractability. This is because we are interested in low-concentration sea ice with strong shear, and so we are less interested in the plastic part of the rheology. The choice of pressure function could be made the same as [4], however it would not change much, since at low concentrations it is similar to our pressure function.

The boundary condition in C used for both the uncoupled and coupled filament model is to impose an outer boundary condition $C(L) = C_\infty$. As will be seen in sections 3 and 4, this choice of boundary condition allows a flux of mass through the domain. Outside the filament there are other processes acting to redistribute sea ice. If these processes act to produce a concentration of C_∞ then it is reasonable to impose this as a condition at the outside of the domain. Additionally, this situation allows us to approximate the case where there is a small filament in a large domain, i.e. a case where $v_w = 0$ for $|y| > l$ and $\partial_y C(L) = 0$. In such a case, the flux through $y = l$ is supplied by the diffusion in the outer boundary. Numerically simulating such a setup can be computationally challenging however, due to the range of concentrations involved. Analysis of this case is currently ongoing.

2.4 Non-dimensionalization

These equations can be non-dimensionalized with:

$$y = \hat{y}Y, v = V\hat{v}, v_w = V\hat{v}_w, u = U\hat{u}, u_w = U\hat{u}_w, \eta = \lambda\hat{\eta}. \quad (2.11)$$

The values for these scales are given in table 2.4, except for λ , which is investigated in section 4. The length scale of 1km is characteristic of motion in the submesoscale [9]. If we use the constraint that the Rossby number is 1, and we assume a latitude of 60N, then we get a velocity scale $V \sim 0.05\text{ms}^{-1}$. The other scales are chosen either from [8] or [4].

Parameter	P_0	V	U	L	Γ_d	h	ρ_w
Value	$5 \times 10^3 \text{ Nm}^{-1}$	10^{-2} ms^{-1}	1 ms^{-1}	10^3 m	$5 \times 10^{-3} \text{ ms}^{-1}$	1 m	10^3 kgm^{-3}

Table 1: Parameters for the Uncoupled Filament problem (e.g. without Ekman divergence): sea ice pressure scale P_0 , across- and along-filament ocean velocities U, V , filament width L , linear drag coefficient Γ_d , characteristic sea ice thickness h , and water density ρ_w .

We can find scalings for the variables t and C by using the equations 2.10. In order for the concentration equation for C to have leading order time dependence, then time must scale advectively with v , e.g.

$$t = \hat{t}YV^{-1}. \quad (2.12)$$

In steady state, it must be the case that $v = 0$. This means that any steady state momentum balance in the y direction must be between the pressure term and the drag term, e.g.

$$C(v^w - v) = \frac{hP_0}{\rho_w \Gamma_d} \partial_y C^\alpha. \quad (2.13)$$

This yields an intrinsic scale for C :

$$\begin{aligned} C &\sim \left(VY \frac{\rho_w \Gamma_d}{hP_0} \right)^{\frac{1}{\alpha-1}} \\ C &\sim (10^{-4})^{\frac{1}{\alpha-1}}. \end{aligned} \quad (2.14)$$

This is an intrinsic concentration scale that we use to scale the concentration $C = C\hat{C}$. If the concentration scale departs greatly from this scale then no steady state balance will be possible. In the limit of low concentration (free ice drift), this corresponds to insufficient ice to provide collisions or a resistive force against the underlying ocean currents. In the limit of high concentrations (packed ice) this represents ice that is unable to be significantly influenced by the ocean currents. For convenience, we include the non-dimensionalized equations here, ignoring the hat symbol hereafter:

$$\begin{aligned} \partial_t C &= -\partial_y(vC,) \\ 0 &= -C(v - v_w) - \partial_y C^\alpha + \lambda \partial_y^2 v, \\ 0 &= -C(u - u_w) + \lambda \partial_y^2 u. \end{aligned} \quad (2.15)$$

3 Sea Ice Dynamics Over Strongly Converging Cyclonic Filaments

3.1 Model formulation

The geometry of the problem is summarized in figure 3.1. If we assume that there is

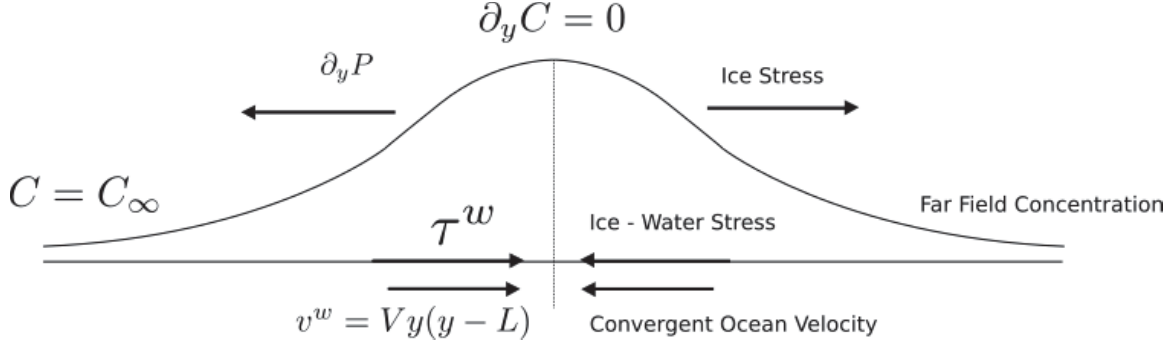


Figure 3.1: Schematic of the of the various forces on acting on the sea ice, the concentration profile that is produced (top line), and the boundary conditions.

no Ekman velocity, and further ignore the viscous term in the y momentum equation (see appendix), we find that the equations become

$$\begin{aligned} \partial_t C + \partial_y(vC) &= 0 \\ 0 &= C(v^w - v) + \partial_y C^\alpha. \end{aligned} \quad (3.1)$$

Doing this allows us to write a single PDE for the concentration (in terms of the dimensionless variables):

$$\partial_t C = -\partial_y(v_w C) + \partial_y^2 C^\alpha. \quad (3.2)$$

We assume that the filament is symmetric on the domain $y \in [-1, 1]$, so that we don't expect there to be any diffusive flux through the center of the domain. Hence we simulate over $0 \leq y \leq 1$ with a symmetry condition

$$\partial_y C(y = 0) = 0. \quad (3.3)$$

Outside of the domain we assume that there are processes unrelated to the filament that maintain the concentrations at some far-field value C_∞ . This leads us to impose the condition

$$C(y = 1) = C_\infty. \quad (3.4)$$

In ongoing work we have also done some analysis using a no flux condition at the outer boundary, although these results will be described elsewhere. We also assume that initially the entire domain is at the far field concentration before the eddy begins applying a stress to the ice, so that

$$C(t = 0) = C_\infty. \quad (3.5)$$

The filament is assumed to have a parabolic structure in the ageostrophic direction, so that in dimensionless form the velocity is

$$v^w = y(y - 1) \quad (3.6)$$

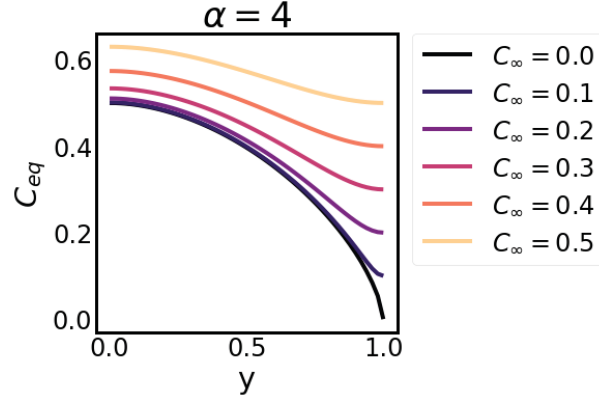


Figure 3.2: Solutions to equation (3.7), for different values of α and C_∞ .

This form is chosen because it satisfies $v(0) = v(1) = 0$ and permits simple analytical steady state solutions.

Equations (3.2)-(3.6) define the system describing the evolution of the sea ice field over the ocean filament.

3.2 Steady state solutions

We can find the steady state solution by integrating (3.1)

$$\begin{aligned}
 0 &= -\frac{d}{dy} \left(Cv^w - \frac{d}{dy} C^\alpha \right), \\
 \int_1^y v^w dy &= \int_1^y \alpha C^{\alpha-1} dC, \\
 C &= \left[\frac{\alpha-1}{\alpha} \int_1^y v^w dy + C(1)^{\alpha-1} \right]^{\frac{1}{\alpha-1}}, \\
 &= \left[\frac{\alpha-1}{\alpha} \left(\frac{y^3-1}{3} - \frac{y^2-1}{2} \right) + C(1)^{\alpha-1} \right]^{\frac{1}{\alpha-1}}
 \end{aligned} \tag{3.7}$$

These solutions are plotted in figure (3.2) for various choices of α and $C(1) = C_\infty$. The results show that the solution tends to flatten when C_∞ is increased. This is consistent with our physical intuition that when the far-field concentration is increased, the diffusivity is increased, and so the solution becomes flatter.

3.3 Transient solutions

We use a simple numerical scheme to simulate the transient evolution to equation 3.2. The advective term is discretized with an upwind advection scheme, and the diffusive term is solved using a second order difference:

$$\partial_t C^i = \frac{C^{i-1} v_w^{i-1} - C^i v_w^i}{\Delta y} + \frac{(C^{i+1})^\alpha - 2(C^i)^\alpha + (C^{i-1})^\alpha}{(\Delta y)^2}.$$

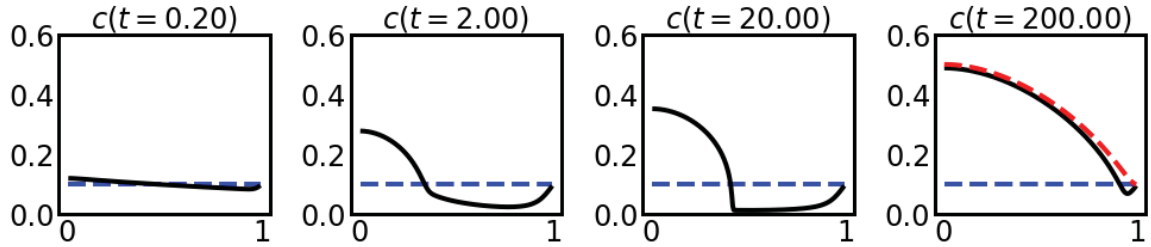


Figure 3.3: Transient evolution of the sea ice concentrations over the uncoupled filament for several exponentially sampled times showing the different stages of evolution. The blue dashed line is the initial condition. The last panel also shows the steady state solution (red dashed line).

The time stepping is done using the `integrate.odeint` routine which is part of the SciPy package (<http://www.scipy.org/>). The exact details of the scheme are unimportant, but it includes both implicit and explicit methods; deciding between an implicit or explicit method with substepping depending on the stiffness of the problem.

The transient solution to equations (2.10) $C_\infty = 0.1$ is shown in figure 3.3. The solution shows that initially the system responds advectively until close to $t = 2$. This is because initially $\partial_y C = 0$, and so there is no diffusion in the system. The result of this early time evolution is shown in the $C(t = 2)$ panel; there is a buildup of concentration in the center of the domain (near $y = 0$), a region of near zero concentrations (between $y = 0.5$ and $y = 1.0$ in the $C(t = 2)$ panel), and a region near $y=1$ which connects the low-concentration region to the boundary condition $C(1) = C_\infty$. This boundary condition has a profound consequence for solutions of our equations. Since there is a non-zero flux through the right hand boundary, the total concentration

$$M = \int_0^1 C dy$$

is not constant in time.

We can think of the evolution of the system as having three distinct stages, an initially advective state where the concentration is redistributed in the system, then an adjustment to equilibrium as M grows larger, and then an approach to the final equilibrium stage (shown in the panel of figure 3.3 corresponding to $C(t = 200)$). These different stages can be visualized by looking at $C(y = 0)$ and M as functions of time, shown in figure 3.4. The initial advective stage happens in the first few time units, and is shown by a rapid change in $C(y = 0)$. This is shown in the $t = 2$ panel. Following this, there is a quasistatic adjustment to the final state, whereby the the central built-up region slowly grows to the edge of the domain due to the flux through the boundary. This happens between approximately times $t = 5$ and $t = 200$. The final adjustment to equilibrium occurs with very little change in either $C(y = 0)$ or M .

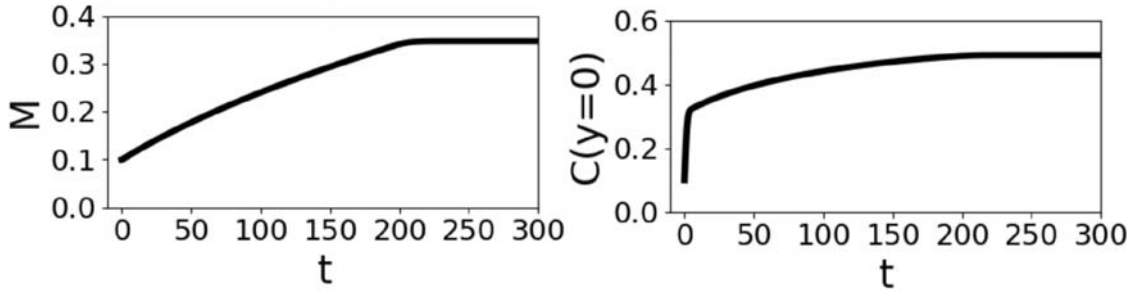


Figure 3.4: The integrated concentration over the domain $M = \int_0^1 C dy$ and the concentration in the center of the filament over the entire simulation, $C(y = 0)$.

3.4 Asymptotic structure

We can understand the slow evolution towards equilibrium by analyzing the concentration equation

$$\partial_t C = -\partial_y q = \partial_y A - \partial_y D \quad (3.8)$$

where $A = -Cv_w$ is the advective component ; $D = -\partial_y C^\alpha$ is the diffusive component; and $q = A - D$ is the total flux of concentration. This is shown in figure 3.5 for a single time in the experiment shown in figure 3.3. We define two lengths: $y = L$ is defined as the point where there is a minimum in $\partial_y C$, and $y = \delta$ is defined as the point in the outer region where $A(\delta) = D(\delta)$. These lines are shown in figure 3.5, and can be used to split the domain into three regions.

The inner region, $0 \leq y \leq L$ contains high concentrations. Since the advection and diffusive flux are close to balancing, the concentrations are changing slowly, and so the profile inside this region can be approximated with the steady state solution. By symmetry, $\partial_y C(0) = 0$, and if we make the approximation that $C(L) = 0$ (e.g. so that the flux at $y = L$ vanishes) we can solve the steady state profile in the region $y \in [0, L]$ up to a choice of constant, equivalent to a choice of $C(0)$. We can choose this constant by requiring the total mass M to match the M from the numerical simulation. This solution is shown as a dashed redline in the upper left panel of 3.5. This is the quasi-steady approximation: at any given time the concentration profile inside this region can be approximated by knowing only the total mass. In this region the fluxes are large, and diffusion can balance advection since the concentration is large. The small residual balance between A and D is what allows the built-up region to accrue mass in time.

In the outer region, $\delta \leq y \leq 1$, the diffusive flux dominates (by definition). The reason for this is $v_w \rightarrow 0$ as $y \rightarrow 0$, but there is no constraint on the diffusive flux. Since $C(1) = C_\infty$, and $\partial_y C(1) \neq 0$, there is a diffusive flux into the domain and a diffusive boundary layer. Immediately away from the outer boundary v_w increases and removes sea ice from the diffusive boundary layer. Since $D \sim C^\alpha$, this decreases the diffusivity and limits the size of the boundary layer.

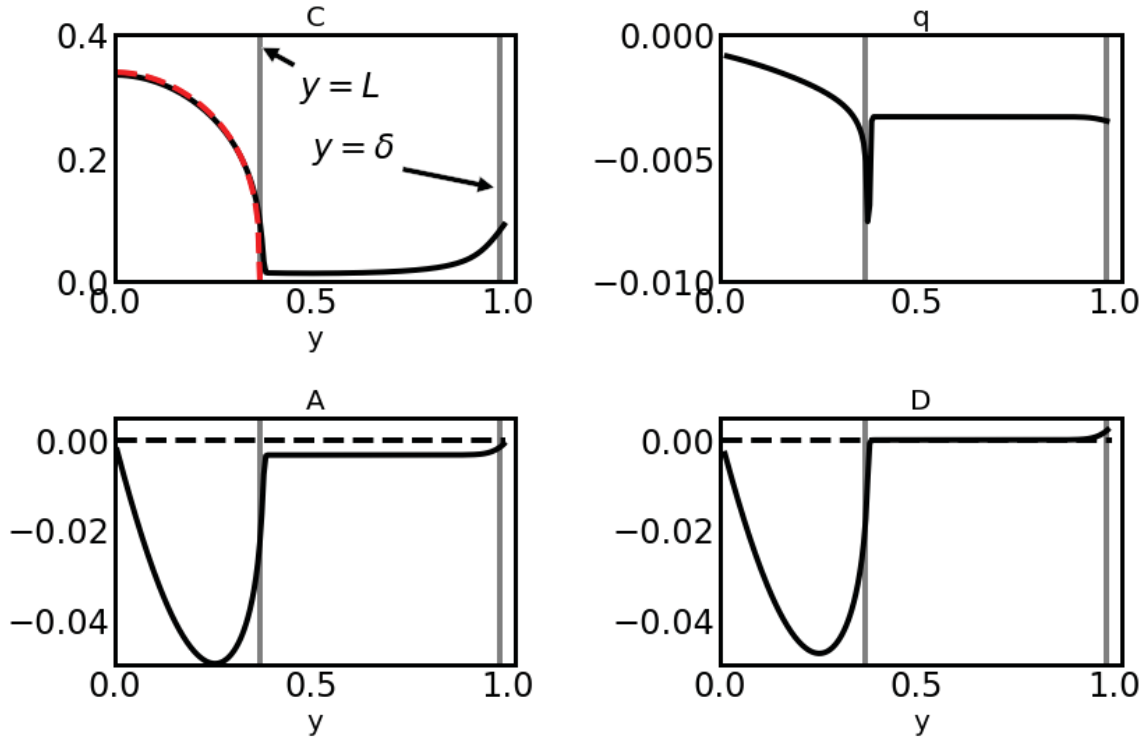


Figure 3.5: The concentration (top left), concentration flux q (top right), advective flux A (bottom left) and the diffusive flux D (bottom right) taken at $t=10$ from the experiment shown in figures 3.3 and 3.4. The red dashed line in the top plot is the steady state solution described in the text. The two grey lines show $y = L$ and $y = \delta$

In the middle region, $L \leq y \leq \delta$, the concentrations are very small, and since $D/A \sim C^{\alpha-1}$, the flux of concentration q is dominated by advection. The advection effectively transfers sea ice from the outer region to inner region without diffusive losses, since the concentrations are low. There is a sharp discontinuity at the left boundary of this region, $y = L$. This is where the regions join, and there is a large growth right at the boundary of the built-up region, which indicates the expansion of the built-up region towards the outer boundary.

Taken together, these observations give an explanation for how the outer boundary fluxes drive the expansion of the central built-up region towards the outer boundary. In the outer region the diffusive flux puts sea ice into the domain, but the advection removes sea ice from this region and advects it through the middle region into the edge, $y = L$ of the central built-up region.

3.5 A heuristic theory for L

Based on the observations in the previous section we can develop a theory for the position of L . We start by assuming that the total mass $M = \int_0^L C(y)dy$ is given. If we approximate $C(L) \approx 0$, then we can calculate L from M , assuming that the system is in a quasi steady state. This gives

$$\frac{dL}{dt} = \frac{\partial L}{\partial M} \frac{dM}{dt}(L) = \frac{\partial L}{\partial M} q(\delta). \quad (3.9)$$

The last line comes from the observation that $dM/dt(L) \approx q(\delta)$ since q does not vary over the interior region. The term $\partial L/\partial M$ can be determined numerically from the steady state solutions. To complete a theory for dL/dt , all we need is a theory for $q(\delta)$.

To determine $q(\delta)$, we start by assuming that δ is quite small, so we can write $v^w \sim \beta\delta$ where β is a shear scale. The advective and diffusive fluxes scale like

$$\begin{aligned} A &= v^w C \sim \beta\delta C_\infty, \\ D &= \frac{\partial}{\partial y} C^\alpha \sim \delta^{-1} C_\infty^\alpha, \end{aligned} \quad (3.10)$$

and since this is the length scale where $A = D$, we can solve for δ , and so find

$$q \sim \beta^{\frac{1}{2}} C_\infty^{\frac{\alpha+1}{2}}. \quad (3.11)$$

We can plot this scaling by doing simulations over a wide range of V and C_∞ , as shown in figure 3.6(a). There is generally good agreement, but for the larger values of C_∞ the values deviate from the prediction. This is not unexpected since for larger C_∞ the inner advective region is not able to develop since the concentrations never become small enough.

We can also use the scaling of (3.11) and (3.9) to propagate L in time. At later times the estimate for L diverges from the value determined by simulating the full system. This is because as the edge of the buildup region approaches the edge of the domain, the scaling theory ceases to apply since there is no longer a clear advective region with small C . The numerical estimate of L also shows some step-like behaviour. This is due to the finite size used for the computational grid.

3.6 Summary

When a parabolic velocity is used, the uncoupled filament equations can be solved for both the steady state as well as for the transient case. The steady state solutions show a strong dependence on the outer boundary concentration condition. The transient solution shows two different timescales. The first is a short advective timescale, which ends when the system is split into three regions; an inner region of high concentrations, a middle region with very low concentrations and an outer diffusive boundary layer. The approach to equilibrium from this state takes a long time because the fluxes from the diffusive boundary layer are limited through the middle region.

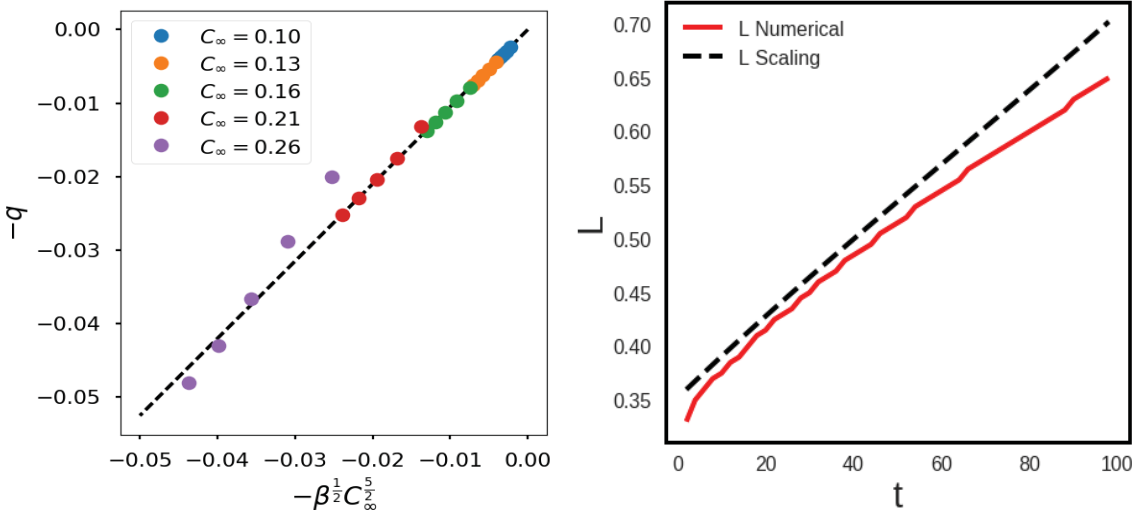


Figure 3.6: (a) Scaling of q given in equation (3.11). (b) $L(t)$ calculated from (3.9) and the numerical solution.

4 Coupled Filament

For a balanced filament or eddy, there will, in general, be no secondary circulation supplied by the ocean that can create convergent motions in the sea ice. The presence of sea ice introduces an additional stress into the system that couples the ice and ocean together by creating an Ekman flow in the surface layer of the ocean. In this section we ask whether this added flow can induce convergent motion of the sea ice, and, if so, what properties does the convergence have that are different from the uncoupled filament? In section 4.1 we introduce the equations, and in section 4.2 we consider some transient solutions. The geometry of the problem is summarized in figure 4.1.

4.1 Equations

For convenience we rewrite equation (2.10) with $v_w = 0$ but with an Ekman velocity v_E (in the non-dimensionalized variables):

$$\begin{aligned}\partial_t C &= -\partial_y(vC) \\ 0 &= -C(v - v_E) - \partial_y C^\alpha \\ 0 &= -C(u - u_w) + \lambda \partial_y^2 u\end{aligned}\tag{4.1}$$

where once again we ignore the viscous stress in the equation for v . For the purposes of this work, we treat the case of a filament using cartesian coordinates (rather than working in polar coordinates as would be required for a circular eddy). We assume that v_E can be taken as an average over the depth D of the Ekman layer. Assuming that in this layer the surface stress from the ice balances a Coriolis force, the stress

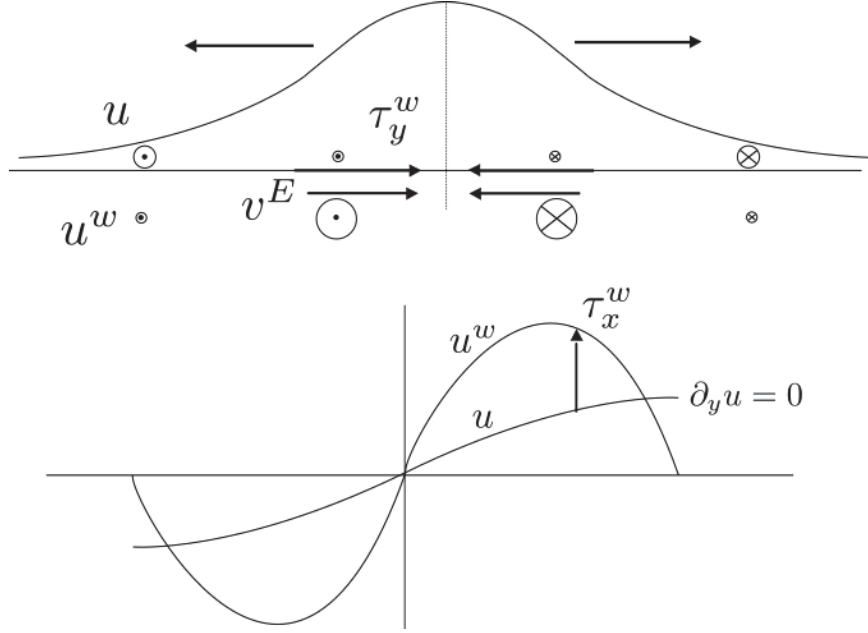


Figure 4.1: Schematic of the of the various forces on acting on the sea ice and the concentration profile (similar to figure 3.1, in a plane (top) and bird's eye (bottom) views. The bottom figure also contains the along filament velocity profile.

in the across frontal direction is

$$\tau_{w,x} = -\rho_w f D v_E$$

Since the drag in the across frontal direction is

$$\tau_{w,x} = C(u - \underline{u}_w)$$

we can write the Ekman velocity in non-dimensional variables as

$$v_E = C(u - \underline{u}_w) \quad (4.2)$$

where we have rescaled V to be $V = UCT/fD$. Note that this velocity scale is very different than in the previous section where we assumed that this velocity scale was supplied by the imposed ocean velocity. We model the geostrophic water velocity \underline{u}_w in a similar way to the ageostrophic component v_w in the previous section and choose

$$\underline{u}_w = y(y - 1), \quad (4.3)$$

in non-dimensional variables.

The addition of equation (4.2) couples the momentum balances in the x and y directions, and hence changes the nature of solving the system in equation (4.1). Before, the equation for the geostrophic velocity u could be ignored in solving the

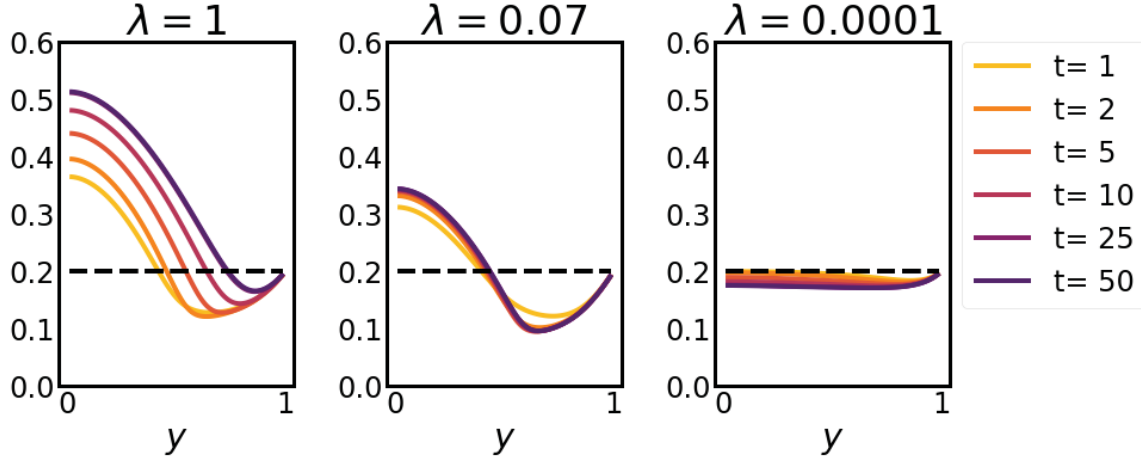


Figure 4.2: C with 3 different values of λ , sampled at various times. The dashed lines show the value of C_∞ for that experiment, 0.2.

rest of the system. We now instead have to solve a boundary value problem to find u , which in turn can be used with C to find v_E . Once v_E is found, this allows v to be determined and used to advance C to a new time step, using the procedure described in the previous section.

Since we now have to solve for u , we have to introduce boundary conditions. We choose

$$u(0) = 0 \quad (4.4)$$

on the basis of symmetry, and

$$\partial_y u(1) = 0, \quad (4.5)$$

equivalent to a no-stress boundary at the edge of the domain. If we did not impose the second condition, then there would be a viscous stress at the edge of the domain that could change the sea ice field outside the domain. Similar to the previous section we choose the boundary condition so that the motion of sea ice inside the domain does not impact outside of the domain.

4.2 Transient solutions

We solve the transient solutions to the system posed in the previous section using a method similar to that in section 3. Now, however, we have to solve the boundary problem associated with u in order to determine v_E before we can timestep C . We do this by using the `solve_BC` package in the `scipy` library (<http://www.scipy.org/>). Briefly, the package uses a collocation method with a cubic spline interpolation of C .

Figure 4.2 shows C for several times and 3 different parameter values of λ . All of the simulations were run for 50 time units. For the smallest value of λ , the total mass of sea ice in the domain decreases by approximately 25% over the simulation and the

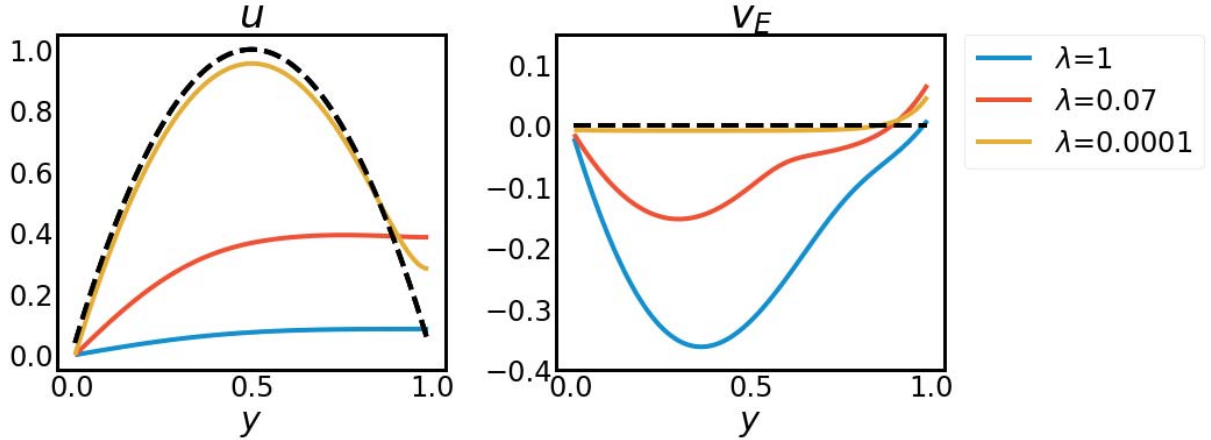


Figure 4.3: u left and v_E right sampled at the end of the experiment show in figure 4.2. In the left figure the dashed black line is the ocean velocity u_W , and in the right figure it is v_E .

profile becomes almost flat. For the largest value of λ , the total mass increases by approximately 60% and the built-up region is able to extend over almost the entire domain. The intermediate value of λ keeps the total mass of ice almost constant over the domain, and has a structure similar to the uncoupled case at short times.

To understand why λ has this control on the total mass and concentration profile inside the domain, we examine profiles of u and v_E taken from the end of the simulation (figure 4.3). In all cases we see that the ice velocity is faster than the ocean velocity near the outer boundary of the domain. The viscous stress is able to spread momentum throughout the domain, and since the outer boundary condition is $\partial_y u = 0$, the momentum is not completely removed from the ice and the ice moves faster than the ocean. By contrast, the inner boundary condition is $u = 0$, and so there is a momentum sink.

For the largest value of λ the ice velocity is very close to 0, and for the smallest λ the ice velocity is very close to the ocean velocity. This matches our intuition, since for a very small viscosity the ice has little viscous resistance and should be moving with the ocean, and for a very large viscosity all of the momentum is transferred to the momentum sink at $y = 0$.

Since $v_E \propto (u - u_W)$, the point where u and u_W cross separates v_E into a positive and negative region. Near the outer boundary $u > u_W$, and so the Ekman transport is actually exporting ice from the eddy into the far field. In the interior of the domain the ice transport is towards the center, and the velocity vanishes at the inner boundary since $u = u_W = 0$. This means that for the largest viscosity there is only a small export of ice near the outer boundary and a strong Ekman transport in the interior. For the smallest viscosity there is a strong export of ice near the outer boundary and a weak convergence in the interior of the domain (since $u \approx u_w$ there). For

the intermediate case the structure of the Ekman transport is not unlike v_w in the uncoupled case.

These differences explain why some parameter values of λ accrue ice in the domain, and others reduce the amount of ice in the domain. For small values of λ , the convergence of v_E is not very strong, and so the system loses some ice mass. This mass loss is eventually stopped because of the diffusive flux across the boundary. For large values of λ , the convergence into the center of the domain is quite strong, and the mass is able to accrue in the center of the domain.

4.3 Summary

The viscous stresses in the ice redistribute momentum in the along-filament direction in such a way that ice near the inner boundary moves slower than the ocean underneath, while the ice near the outer boundary moves faster than the ocean. This creates an Ekman transport that exports sea ice out of the filament near the outer boundary, and pushes sea ice towards the center in the rest of the domain. Strongly viscous sea ice is able to create large Ekman transports that accrue ice over top of the filament because of the large difference between the ice and water velocities. Weakly viscous sea ice is only able to create a weakly convergent Ekman transport and exports ice into the far field. This implies that understanding sea ice rheology in this regime will be important for constraining the ability of eddies and filaments to self-accrue ice.

5 Ramifications for Estimating Surface Ocean Convergences from Sea Ice Concentrations

The previous two sections have discussed two one-dimensional models of sea ice and ocean interaction. In this section we discuss the implications of these models for doing inversions to determine upper ocean velocity from sea ice concentration fields. The main challenges of doing inversions from single sea ice images are:

1. Is there a large difference between $C(0)$ and C_∞ ? If not, the concentration buildup will not be detectable from the background.
2. Does the system reach an equilibrium on a timescale similar to or shorter than the persistence timescale of ocean flows (approximately 5 days)? If not, then we need time dependent information to properly constrain the flow and so will not be able to do so from a single image.

Here we try to recast the results from previous sections in terms of these questions and try to provide some heuristic criteria about which conditions will be suitable for inversions.

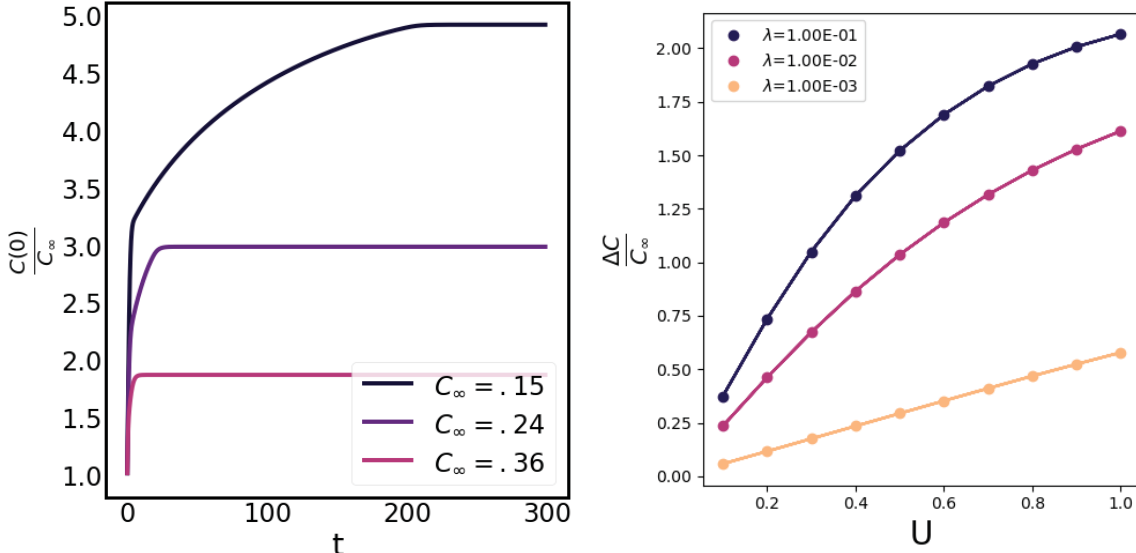


Figure 5.1: (a) Time series of the signal-to-background ratio $C(0)/C_\infty$ for different values of C_∞ , from the uncoupled model. (b) $[C(0) - C_\infty]/C_\infty$ for different values of λ and the forcing velocity scale (U) after 5 time units (~ 5.8 days). for the coupled model

5.1 Timescales for uncoupled inversions

To answer the above questions we compute the signal-to-background ratio $C(0)/C_\infty$, which quantifies the concentration buildup in the center of the domain compared with the outer boundary. This is shown for several boundary conditions in figure 5.1. Two timescales are clearly visible: there is a sharp increase for $t < 1$, and then a second longer timescale with a smaller increase. For large values of C_∞ there is a small signal-to-background ratio over the entire time. This means that the steady state solution will be a good approximation to the time-dependent solution, since the period of transience is relatively small and the solution quickly converges to the steady state.

These results yield two rules of thumb:

1. Low background concentrations give higher signal-to-background ratios, which means that inversions will be able to be computed more accurately. This also means that packed ice ($\sim 100\%$ concentration) are unlikely to be invertible, even without taking account of any plastic part of the rheology [4].
2. The fast time scale of the sea ice adjustment means that the ice concentration will be approximately in balance with the ocean forcing on short (5-10 day time scales).

5.2 Timescales for coupled inversions

For the coupled system, the solutions evolve in a much more complicated manner compared with the uncoupled system. If there were a non-monotonic relationship between the strength of the forcing velocity U and the other system parameters, then the system will no longer be invertible. We test whether or not this is the case in figure 5.1 by calculating the enhancement of the sea ice concentration over the center of the filament for various U and λ . We find a monotonic relationship between the enhancement and the scale of the forcing velocity when λ is fixed, although the relationship is strongest for the stronger sea ice.

This suggests the following simple observations:

1. Higher viscosity allows a stronger coupling between the ocean currents and the sea ice concentrations.
2. There is an approximately monotonic relationship between the scaling of the ocean velocity and the enhancement of sea ice above.

Together, these results suggest that it may be possible to invert submesoscale currents from observations of ice concentration. Note that this result was not guaranteed, nor obvious a priori. There are many ways that this model could have failed to validate the hypothesis that inversions would be possible. The adjustment timescales between the ice and the ocean could have been too different, or the enhancement of sea ice in the center of the domain could have been too low to be meaningful. However our results suggest that the fast adjustment timescale associated with advection of low concentration sea ice allows ocean forcing to enhance sea ice concentration over convergent ocean currents. Future studies could analyze models with more realistic rheologies, or attempt simple inversion methods on data from realistic ice-ocean circulation models.

6 Conclusions

In the marginal ice zone, ocean filaments are able to accrue significant sea ice. In this study we have considered two idealized test cases. We first considered an uncoupled filament, where the surface ocean currents create a convergence of ice over the filament. We find that there are two timescales. The first is a short advective timescale that is able to accumulate sea ice into a built-up region over the filament in a few days. The second timescale can take several hundred days, and is related to a diffusive boundary layer (where the diffusion is controlled by internal ice stresses providing a driving force to redistribute ice mass). We have developed a simple theory to calculate the scaling of the diffusive flux and shown how it can be used to propagate the boundary of the built-up region near the center where the sea ice concentration is in quasi-steady equilibrium.

We also considered a coupled filament, where we assume that the surface currents are non-divergent, but the ocean boundary layer is coupled to the ice stress through Ekman transport. The viscous stress spreads ice velocity in the along-filament direction so that the ice near the outer boundary of the filament is moving faster than the ocean underneath. This results in an Ekman transport that exports sea ice through the outer boundary but also has a convergent section pushing sea ice towards the inner section. We show that in this case the ability of the filament to accumulate sea ice is strongly dependent on the strength of the ice viscosity. When the ice viscosity parameter is very large, there are strong convergent velocities at the ocean surface. When the ice viscosity parameter is very small, the convergent velocity is small. This idealized study shows that both the uncoupled and coupled filaments are able to accumulate significant amounts of sea ice on oceanographically relevant timescales. These results suggest that ocean turbulence statistics can be inferred from still satellite images of sea ice in marginal ice zones.

Appendix: justification for ignoring the viscous term in the uncoupled filament

The Hibler model [4] assumes that the viscosity is

$$\nu = \max, \left(\frac{1}{E^2} \frac{P}{\max(e_{min}, |\underline{e}|)}, \nu_{min} \right) \quad (6.1)$$

where

$$|\underline{e}| = \frac{1}{\alpha} \sqrt{2\text{tr}(\underline{e} \cdot \underline{e}) + (E^2 - 1)[\text{tr}(\underline{e})]^2} \quad (6.2)$$

is the strain invariant associated with an elliptical yield curve of eccentricity $E = 4$, with the strain rate tensor $e_{ij} = \frac{1}{2}(\partial_i u_j + \partial_j u_i)$.

If we assume that the geostrophic velocity is larger than the ageostrophic velocity, but that both vary over the same spatial scale, then we find that

$$|\underline{e}| \sim \frac{U}{L}. \quad (6.3)$$

For the purposes of this scaling, we will be interested in only the part of the viscosity that does not involve e_{min} and ν_{min} . We ignore ν_{min} because we are interested in the largest values of ν and ignore e_{min} because this value is much smaller (by a factor of 10^6) than U/L (from the parameters listed in table 1).

The viscosity then scales like

$$\nu \sim \frac{PL}{U}, \quad (6.4)$$

so the ratio of the pressure gradient force to the viscous force in the along-filament direction is

$$\frac{\partial_y (\nu \partial_y v)}{\partial_y P} \sim \frac{V}{U} \quad (6.5)$$

which we assume to be small.

Acknowledgments

I would sincerely like to thank Georgy Manucharyan, Andrew Wells, and Sam Pegler for their time and guidance through this project. I would also like to thank Mary-Louise Timmermans and Claudia Cenedese for organizing the summer school, and my fellow fellows for their companionship.

References

- [1] E. ABRAHAMSEN, *Sustaining observations in the polar oceans*, Philosophical Transactions of the Royal Society A, 372 (2014), p. 20130337.
- [2] T. W. ARMITAGE, S. BACON, A. L. RIDOUT, S. F. THOMAS, Y. AKSENOV, AND D. J. WINGHAM, *Arctic sea surface height variability and change from satellite radar altimetry and grace, 2003–2014*, Journal of Geophysical Research: Oceans, 121 (2016), pp. 4303–4322.
- [3] D. L. FELTHAM, *Sea ice rheology*, Annual Review of Fluid Mechanics, 40 (2008), pp. 91–112.
- [4] W. HIBLER III, *A dynamic thermodynamic sea ice model*, Journal of Physical Oceanography, 9 (1979), pp. 815–846.
- [5] E. HUNKE AND J. DUKOWICZ, *An elastic–viscous–plastic model for sea ice dynamics*, Journal of Physical Oceanography, 27 (1997), pp. 1849–1867.
- [6] P. KLEIN AND G. LAPEYRE, *The oceanic vertical pump induced by mesoscale and submesoscale turbulence*, Annual Review of Marine Science, 1 (2009), pp. 351–375.
- [7] V. LYTLE, R. MASSOM, A. WORBY, AND I. ALLISON, *Floe sizes in the east antarctic sea ice zone estimated using combined sar and field data*, in Space at the service of our Environment, 1997, pp. 931–936.
- [8] G. E. MANUCHARYAN AND A. F. THOMPSON, *Submesoscale sea ice-ocean interactions in marginal ice zones*, Journal of Geophysical Research: Oceans,(2017).
- [9] J. C. MCWILLIAMS, *Submesoscale currents in the ocean*, 2016.
- [10] J. A. MENSA AND M.-L. TIMMERMANS, *Characterizing the seasonal cycle of upper-ocean flows under multi-year sea ice*, Ocean Modelling, 113 (2017), pp. 115–130.
- [11] B. RALLABANDI, Z. ZHENG, M. WINTON, AND H. A. STONE, *Formation of sea ice bridges in narrow straits in response to wind and water stresses*, Journal of Geophysical Research: Oceans, (2017).
- [12] M. C. SERREZE AND R. G. BARRY, *The Arctic climate system*, Cambridge University Press, 2014.
- [13] M.-L. TIMMERMANS AND P. WINSOR, *Scales of horizontal density structure in the chukchi sea surface layer*, Continental Shelf Research, 52 (2013), pp. 39–45.
- [14] J. A. WHITEHEAD, *Dimensions of continents and oceans–water has carved a perfect cistern*, Earth and Planetary Science Letters, 467 (2017), pp. 18–29.